# LONG-TERM RATE OF EARTHQUAKE RUPTURES IN COMPLEX FAULT SYSTEMS.

F. VISINI[1], A. VALENTINI[2], T. CHARTIER[3,4], O. SCOTTI[4], B. PACE[2]

[1]Istituto Nazionale di Geofisica e Vulcanologia, L'Aquila, Italy

[2]Univeristà degli Studi di Chieti-Pescara Disputer Department, Chieti, Italy

[3]Ecole Normale Supérieure de Paris, Geosciences Department, Paris, France

[4]Institut de Radioprotection et Sûretét Nucléaire, Paris, France

*E-mail contact of main author: francesco.visini@ingv.it*

**Abstract**. Use of faults in seismic hazard models allows capturing the recurrence of large-magnitude events and therefore improve the reliability of probabilistic seismic hazard assessment (PSHA). In the past decades, fault segmentation provided an important framework for quantifying fault-based PSHA. However, in the last years, complex coseismic ruptures (e.g. 2010 M 7.1 Canterbury, 2012 Mw 8.6 Sumatra, 2016 Mw 7.8 Kaikōura, 2016 Mw 6.5 central Italy) imposed to pay particular attention to the treatment of all possible combinations of rupture scenarios for PSHA. Here we present two methodologies to model rate of ruptures along fault systems, one based on a floating rupture approach (FRESH) and another one based on assumed rupture scenarios (SUNFISH). They represent alternatives to SHERIFS, an approach recently proposed to go one step beyond the strictly-segmented one commonly used in Europe. Differences in the three approaches are related to the way slip rate, rupture geometries and MFD are modelled. To quantify differences between the three methodologies, we compared PSHA results based on geometries and slip rates of a fault system located in NE Italy, assuming a specified maximum magnitude and the same seismic moment rate target. Differences of up to 20-30% in the resulting hazard levels are observed. Finally, we demonstrate that the three methodologies are able to solve for the long-term rate of ruptures with resulting PSHA that reflect the fault system geometry and slip rates, without any assumption on segment boundaries. Using fault-based approaches in PSHA requires collecting as much local geological information as possible. Now that multi-fault rupture approaches are available, simplistic, uniform slip rate approaches along complex fault systems should be avoided to the benefit of local data collection, which should be strongly encouraged (fault slip rates should be locally evaluated, fault geometries should be studied).

**Key Words**: fault system, slip rates variability, long-term rate of ruptures, PSHA

## 1. INTRODUCTION

Use of faults in seismic hazard assessment allows to capture the recurrence of large-magnitude events and therefore to improve the reliability of probabilistic seismic hazard assessments (PSHA). From a seismic hazard point of view, the first step is, ideally, to identify the potentially active faults and then to evaluate the rate of earthquakes that each fault may generate.

In the past decades, fault segmentation provided an important framework for quantifying fault-based PSHA (e.g., [1]; [2]; [3]; [4]; [5]). Various features were proposed as potentially factors that control the location and length of rupture (i.e., rules for segmentation). For example, [6] proposed that rupture could be limited to regions between bends in faults and terminated at geometric barriers defined as conservative or non-conservative, depending on the shape of the barrier. One of the first segmentation models was proposed by [7] for the Wasatch Fault (Utah, USA); they suggested six segments on the basis of homogeneous fault properties and historical seismicity and as many as 10 segments based on the geometric change along the fault. Later, [8] defined the concept of characteristic earthquake model, in which "seismic-energy release

on a given segment occurs mostly as earthquakes of a size that is characteristic of the segment". The main assumption behind segmentation and the later characteristic earthquakes model was that coseismic ruptures would rupture an entire segment but would not rupture onto adjacent segments. In this framework, a segment represents a fault or an ensemble of faults that repeatedly slipped together during past single events and likely will show the same behaviour during the next future earthquakes. More recently, [5] have rather explored the geological, geometrical and kinematical constraints that may allow ruptures to jump from one fault to the next, hereafter named FtF rupture. Factors that have been used to allow or impede FtF rupture scenarios are: (i) fault gaps among aligned structures; (ii) intersections with cross structures (often transfer faults) significantly extending along strike and oriented at nearly right angles to the intersecting faults; (iii) overlapping or underlapping en echelon arrangements with significant separations between faults; (iv) bending greater than a certain angle for a significant length; (v) average slip rate variability along a strike greater than or equal to 50 %; and (vi) significant changes in seismogenic thickness among aligned structures. The latest Californian earthquake rupture model (UCERF-3) developed a novel methodology to treat all possible combinations of rupture scenarios within the same branch of the logic tree ([9]). In their terminology, faults are divided into smaller sections and all possible section-to-section ruptures are investigated. The possibility of ruptures happening is controlled by a set of geometric and physical rules and the rate of earthquakes is computed using a "grand inversion" of the seismological, geological, paleoseismological and geodetic data available in California. The regional Gutenberg-Richter magnitude-frequency distribution of earthquakes in California and the geodetic deformation rate are used as a target for the total earthquake rupture forecast in each deformation model. However, this approach is possible only where a large amount of data is available.

Actually, for many fault networks, only sparse seismological and geodetic data are available and the geological record is often the most detailed source of information concerning the faults' activity. Furthermore, nature has already shown to us that FtF rules should be considered with caution, as testified by the very complex coseismic ruptures observed during the 2012 Mw 8.6 Sumatra offshore earthquake ([10]), the 2010 Mw 7.1 Dartfield/Christchurch earthquake ([11]), the Mw 6.5 2016 ([12]) earthquake in central Italy, and the 2016 Mw 7.8 Kaikōura earthquake ([13]). In order to develop a methodology that allows building seismic hazard models controlled by geologic/geodetic estimated fault slip rates, [14] proposed a novel methodology that, similarly to UCERF-3, considers FtF ruptures as an aleatory uncertainty but without relying on a grand inversion. Rates of earthquakes on faults are then computed following two constraints: the magnitude-frequency distribution (MFD) of earthquakes in the fault system as a whole must follow an imposed shape and the rate of earthquakes on each fault is determined by the specific slip-rate of each segment depending on the possible FtF ruptures each segment is involved in. In their methodology, FtF ruptures follow a rule to be specified by the user. Therefore, the main assumptions of their method are (i) the set of rupture scenarios as a list of the possible FtF ruptures in the fault model (several lists of FtF can be explored as different branches of a logic tree) and (ii) the shape of the regional MFD target.

The initial work of [14] raised discussion in the framework of the European Seismological Commission Fault2SHA Working Group activities (hereinafter Fault2SHA, https://fault2sha.net), aimed at sharing ideas and comparing methods in order to improve fault-based PSHA through interaction with earthquake geologists, seismologists and geodesists. The

fruitful discussions led to the development of two additional alternative approaches to model FtF rupture and to estimate long-term rates of occurrence of earthquakes along faults.

In this paper we compare PSHA results based on these three approaches developed within the Fault2SHA using the geometries and slip rates provided in an available seismogenic source database (DISS 3.2.0, http://diss.rm.ingv.it/diss/, DISS hereinafter) for the faults of the Montello fault system (northeast of Italy) and assuming a specified maximum magnitude and seismic moment rate. We also compared the above approaches with a strictly-segmented approach, using data of the individual seismogenic sources listed in the DISS, and with a model based on a simple assumption in which we assumed an average slip rate along a composite seismogenic source. The aim of these comparisons is to show how PSHA is affected along the fault when we include slip rate variability along the strike of an investigated fault. The two approaches here proposed (namely, SUNFiSH and FRESH), and the published SHERIFS method ([14]), even if based on different assumptions, all aim to evaluate the long-term rate of occurrences of earthquake ruptures. It is worth noting that the aim here is to understand the differences in the three approaches and how the assumptions impact the PSHA results.

## 2. The test case area – the regional context

The chosen area where we carried out a PSHA methodological comparison is located in the NE of Italy, in the Veneto-Friuli Alpine region, between the Italian-Slovenian border to the east and the Lessini mountains to the west (Fig. 1). This area is characterized by the presence of WSW–ENE to WNW–ESE trending low-angle thrusts also known as Eastern South-alpine Chain (ESC), a SSE verging thrust belt ([15]; [16], [17]). As testified by historical and instrumental seismicity, and by geodetic studies that estimate N–S shortening rates on the order of 2 mm/yr (e.g. [18] in the epicentral area of the 1976 Friuli earthquake sequence, mainshock Mw 6.5), this area is still seismically active. During the last ~ 700 years, this sector has been struck by several moderate to large earthquakes as reported in the Parametric Catalogue of Italian Earthquake 2015 (CPTI15, [19]). Eight earthquakes of Mw higher or equal 6.0 occurred in this time window: 1511-03-26 (Mw 6.3; Io IX); 1695-02-25 (Mw 6.4; Io X); 1794-06-07 (Mw 6; Io VIII-IX); 1928-03-27 (Mw 6 IX); 1936-10-18 (Mw 6.1; Io IX); 1976-05-06 (Mw 6.5; Io IX-X); 1976-09-15 (Mw 6; VIII-IX) as well as numerous earthquakes with magnitude between 5 and 6, both historical and instrumental. As suggested by the fault plane solutions of instrumental earthquakes and by the 1976 seismic sequence, the seismic activity of the case study area is almost totally controlled by the compressional sources still active today ([20]; [21]). These sources are fully described in the DISS. Based on structural and geomorphological observations and by the association of the distribution of the intensity data points of the strong historical earthquakes with source geometry and position, the DISS proposed a segmentation of the external front of the ESC (Fig. 1). However, in this area, the identification of individual seismogenic sources is not an easy task due to the structural configuration of the thrust belt, the low strain rates and the low-angle thrusts that do not reach the surface. Given the uncertainties in the input data concerning the actual segmentation, it is important to provide an un-segmented fault approach to go beyond the segmentation issue, in regions affected by similar uncertainties as the ones described above.

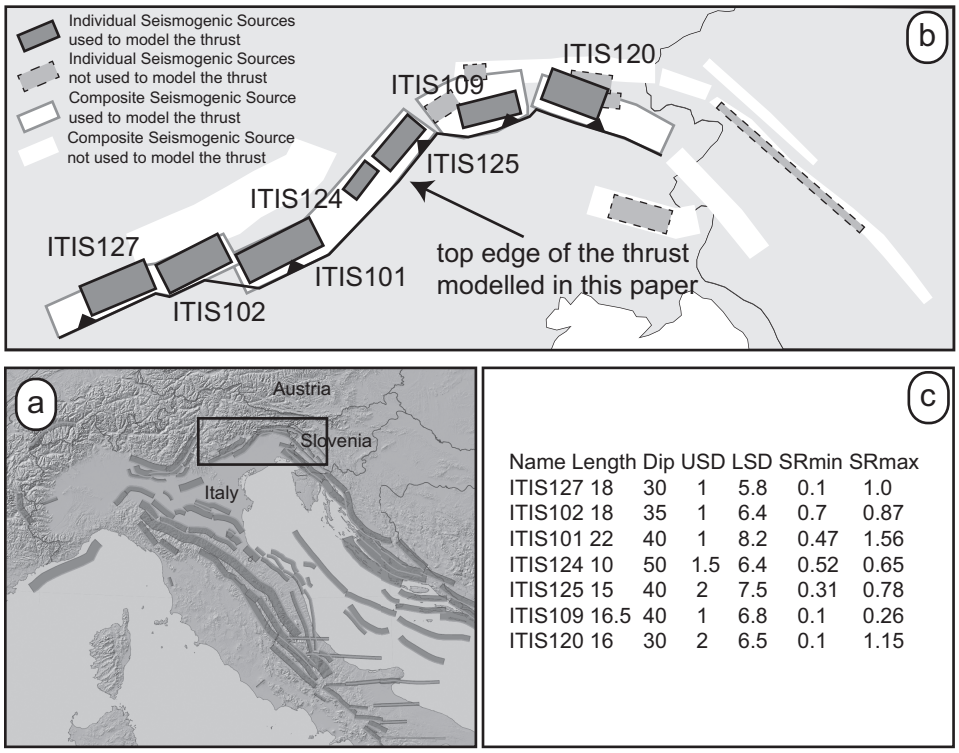


*FIG. 1. 1a) Location map of Figure 1b, with the composite seismogenic sources available in the DISS. 1b) Main thrust and seismogenic sources in the testing area: individual and composite seismogenic sources used or not-used to model the fault system geometry, basing on the DISS. c) parameters of the individual seismogenic sources used to model the fault system geometry: Name is the identification code; Length is length long strike (km); Dip is the dip angle; USD is the upper seismogenic depth (km); LSD is the lower seismogenic depth (km); SRmin and SRmax are, respectively, the lowest and the highest value of the range of slip rate (mm/yr). All these data are from DISS.*

## 2.1 The test case area - Input data

Four composite seismogenic sources (CSS) published in the DISS are considered in this paper: ITCS007, ITCS060, ITCS062 and ITCS066 (Fig. 1). All CSSs are characterised by a thrust tectonic regime. In the DISS approach, a CSS represents a crustal seismogenic source zone containing an unspecified number of seismogenic sources that cannot be singled out ([22]), to which a slip rate (with uncertainty), a maximum magnitude (Mmax), and other geometric and kinematic parameters are associated by expert opinion.

Based on the geometry and slip rate information available in DISS (Fig. 1), we defined geometrical and kinematic parameters that serve as common inputs to the 3 multi-fault rupture approaches:

- fault trace and length along strike (~180 km) is the same for all the approaches;
- the dip angle varies along the strike of the fault system; each approach has a procedure to treat this variability (details in section 3);
- upper seismogenic depth is 1 km for all the approaches;
- lower seismogenic depth varies between 7 km and 9 km; each approach has a procedure to treat this variability (details in section 3);
- rake is the same for the 3 approaches (the kinematics is pure thrusting);

- Mmax is the same for all the approaches;
- slip rate inputs are the same for all the approaches, but each approach has a procedure to convert slip rates into activity rates;
- a regional b-value is the same for the 3 approaches;
- total seismic moment rate is the same for the 3 approaches.

Fault trace, dip angles, upper and lower seismogenic depths and rake are derived from the DISS; in the following, we illustrate the procedure followed to define Mmax, slip rates, b-value and total seismic moment rate.

The starting point for defining slip rates were the values listed in the DISS (Fig. 1), associated with the individual seismogenic sources. Specifically, in the DISS, these slip rates were derived from throw rates calculated using the depth of the base of Quaternary (i.e. Calabrian 2 Ma) recognized in the foot-walls of the thrust, ([17]), considering a mean dip angle of the faults, and from geodynamic constraints like GPS deformation velocities where geological and geomorphological data were not available (details in [23]). For each individual seismogenic source, we computed a mean of the range given in Fig. 1, this means is representative of the slip rate along the strike of that individual seismogenic source. Successively, slip rates of the individual seismogenic sources were interpolated to define a profile of slip rate along the strike of the fault system. Individual slip rates and profile are shown in Fig. 2a. The profile of slip rate is the input for the 3 approaches (SUNFiSH and FRESH) here proposed as well as for SHERIFS. In this study, we also compared these three un-segmented approaches with a strictly-segmented approach, which used data of the individual seismogenic sources listed in the DISS, and with a model based on a simple assumption in which we assumed an average slip rate along a composite seismogenic source.

Details on the procedures to convert slip rates into activity rates, as well as on how the input data (slip rate of individual seismogenic sources and profile) was used, are given in the following sections.

To calculate the b-value of the MFD, we applied the maximum-likelihood method of [24] to the historical earthquake of the CPTI15, with the magnitude completeness intervals evaluated by [25]. We obtained a b-value equal to 0.99, that served as input for computing MFD considered by the 3 approaches either for the individual ruptures (SUNISH/FRESH) or for the region as a whole (SHERIFS).

To evaluate the maximum magnitude, we applied a regression relationship based on the concept of aspect ratio, i.e. the ratio between down-dip width and along-strike length, and from scaling relationship between subsurface total length and moment magnitude ([26]). The used aspect ratio relationship ([27]) allows determining the maximum possible rupture length (Lar: Length from Aspect Ratio) in a source of well-constrained seismogenic thickness. In this case, assuming a value of seismogenic thickness of ~7 km, a dip angle of 30° and applying the aspect ratio relationship in [27]:

$$Lar = -2.3725 + 1.9354 \cdot (\sin(\text{dip angle}) \cdot \text{seismogenic thickness}) \quad (1)$$

we obtained a Lar of ~ 24 km. Then, by applying scaling relationship between rupture length at depth and Mw [26], we computed a maximum magnitude of Mw 6.5. This Mmax value is considered as the maximum possible rupture scenario that can occur on this fault system.

Lastly, we determined a target value for the moment rate ($\dot{M}_{ot}$), to be used as a common data for the 3 methods. The seismic moment rate was directly calculated in SHERIFS from the slip-rate, the area and the shear modulus of the faults. This moment rate value of 3.29E+16 $Nmyr^{-1}$ calculated by SHERIFS was then used as input for SUNFiSH and FRESH. As a matter of fact, having unique b-value, Mmax and seismic moment rate, differences in the resulting PSHA only depend on the procedures to determine the activity rates.

## 3. New approaches to evaluate long-term rate of every possible earthquake rupture.

This paper presents two new objective and reproducible methodologies able to include FtF and slip rate variability along strike (and possibly with depth) of a fault, or of a fault system, into the modelling of earthquake occurrences. Integrating geo-morphological data, geodesy and historical and paleo-seismological data, the likely rupture history of the fault over a long period, including more than a seismic cycle, could be determined. Reconstructing the seismic cycle and the possible time-and-space variations of earthquake occurrences along a fault system is ideal for a better evaluation of PSHA, however this is actually possible only for a few case studies (e.g., [28]; [29], 2010; [30]) or with numerical simulations (e.g., [31]; [32]; [33]). Instead, it is worth noting that, often, slip rate along faults are extrapolated from a few measurements along a fault system, and where these measurements are derived by paleoseismological data, can be representative only of a limited earthquake history related to a few large events. To better illustrate this concept, and show how to manage such fault data for PSHA purposes, we applied both methods to the thrust fault system located in north-east of Italy previously described. Results from these two approaches were compared with a published FtF method (SHERIFS by [14]) and with two new approaches using a strictly-segmented and an un-segmented-uniform-slip rate approach. The three approaches are described in the following sections. It is important to note that both methodologies here presented, as well as the SHERIFS approach used for comparison, are extensible to a potentially more complex network of faults, however, to exemplify the methodologies, we used only the geometries and parameters of the 7 sources highlighted in Figure 1.

### 3.1 SUNFiSH: a sub-sectioning approach

The method described in this section allows solving for the long-term rate of every possible earthquake rupture, above a threshold magnitude, on a fault system. With this method, hereinafter called SUNFiSH (*SUbsectioNs of Fault in Seismic Hazard*), we subdivide the entire length of the fault system into n equal-length subsections (Fig. 2a). Following the rules proposed in UCERF3 ([9]), the length of each subsection is about half of the down-dip width, and the minimum rupture length is approximately equal to the seismogenic thickness (a rupture must contain at least two adjacent subsections). A rupture can only jump to a neighbour subsection. If the minimum rupture length is given by the seismogenic thickness, the maximum rupture length is given by the maximum magnitude of 6.5 (previously described in section 2) that means a ~ 24 km rupture surface length which in turn means that the maximum rupture length must contain at most 7 adjacent subsections. In the test case, SUNFiSH accounted for ruptures that involved from 2 to 7 adjacent subsections, that yielded 291 possible combinations (ruptures), summarized in Table 1.

| number of subsections involved | number of possible scenarios | Length (km) | Mmax |
|---|---|---|---|
| 2 | 51 | 7 | 5.8 |
| 3 | 50 | 10.5 | 6.0 |
| 4 | 49 | 14 | 6.2 |
| 5 | 48 | 17.5 | 6.3 |
| 6 | 47 | 21 | 6.4 |
| 7 | 46 | 24.5 | 6.5 |

*TAB. 1. Number of sub-sections and number of possible scenarios, Mmax and length along strike modelled by SUNFiSH*

The second step is to assign to each rupture a slip-rate value, to this aim SUNFiSH uses a slip rate profile, and computes an average slip rate for the *i*th rupture (*Vi*) by means of the mean value theorem for integrals:

$$Vi = \frac{1}{b-a}\int_a^b f(t)dt \qquad (2)$$

where *f(t)* is the function that interpolates the slip rate profile, and *b* and *a* are the tips of the *i*th rupture (Fig. 2a). The theorem states that a continuous function on a closed, bounded interval has at least one point where it is equal to its average value on the interval. In SUNFiSH, the continuous function is given by the interpolation of the slip rate profile (Fig. 2a, b) and the values of the closed and bounded interval are the slip rate values at the tips of a given rupture.

SUNFiSH attributes to each subsection the dip angle and seismogenic thickness of the closest fault, starting from the fault system given in Figure 1c. Then to evaluate the dip angle and seismogenic thickness of each rupture, SUNFiSH computes average values of the subsections' parameters involved in the rupture. Future implementations will include complex fault geometries at depth as well.

Once each rupture is characterized in terms of length, dip angle, seismogenic thickness and slip rate, SUNFiSH requires calculating a budget of seismic moment rate for each rupture. According to [34], the budget of seismic moment rate allowed by each rupture is given by the seismic moment of the Mmax divided by the mean recurrence time of the Mmax. In this case, Mmax is the maximum magnitude of each rupture, and it is worth noting that it is lower or equal to the Mmax evaluated for the fault system (Mw 6.5); values of Mmax of the ruptures, given the number of subsections involved in a rupture, are listed in Table 1. To evaluate the Mmax of each rupture, we relied on the FISH tool (http://fish-code.com) which computes normal probability density functions for three Mmax estimates: an Mmax based on the calculated scalar seismic moment (*Mo*) and the application of standard formula [35] formula, with a standard deviation of 0.3 ([34]) and two Mmax magnitudes and associated standard deviations estimates by applying [26] empirical relationships for the maximum subsurface rupture length and maximum ruptured area. An Mmax and the associated standard deviation are obtained (Table 1) by summing these 3 probability density functions.

The budget of seismic moment rate for each ith rupture was obtained by:

$$\dot{M}_0 i = \mu LiWiVi \quad (3)$$

Where *Li* and *Wi* are, respectively, the length along strike and along the dip of the *i*th rupture, $\mu$ is the shear modulus and *Vi* is the average slip rate (eq. 1) of the *i*th rupture. The seismic moment rate of the *i*th rupture (eq. 3) is then scaled by:

$$\dot{M_{0si}} = \dot{M}_{0i} * \frac{\dot{M_{ot}}}{\sum \acute{M}_0 i} \quad (4)$$

where $\dot{M}o_i$ is the annual seismic moment rate of the ith rupture, and $\dot{M}_{ot}$ is the annual seismic moment rate target, the latter defined in section 2.

Finally, we calculated the MFDs for each rupture. To compute the seismic activity rates, we assumed a classical Gutenberg-Richter model (GR), and the rates of expected seismicity (Fig. 2c) for each rupture are determined as follows:

$$log_{10}N_{(M)} = a - bM \;\; with M_t \leq M \leq M_{max} \quad (5)$$

where *N(M)* is the number of earthquakes with a magnitude greater than or equal to the lower threshold magnitude of the distribution (*Mt*) and less than or equal to the Mmax of each rupture (Table 1), b was assumed equal to 0.99 (see section 2), and a is the logarithm of the number of earthquakes with *M* >= 0. *Mt* was chosen equal to 5.5 because this is a threshold of the geological detection of the causative faults of these intermediate size earthquakes (e.g. [36]). The a value is computed for each rupture balancing the total expected annual seismic moment rate with the $\dot{M_{0si}}$ obtained with equation 4 (Fig 2c). The impact on seismic hazard due to the use of various shapes of the MFD is beyond the scope of this paper.

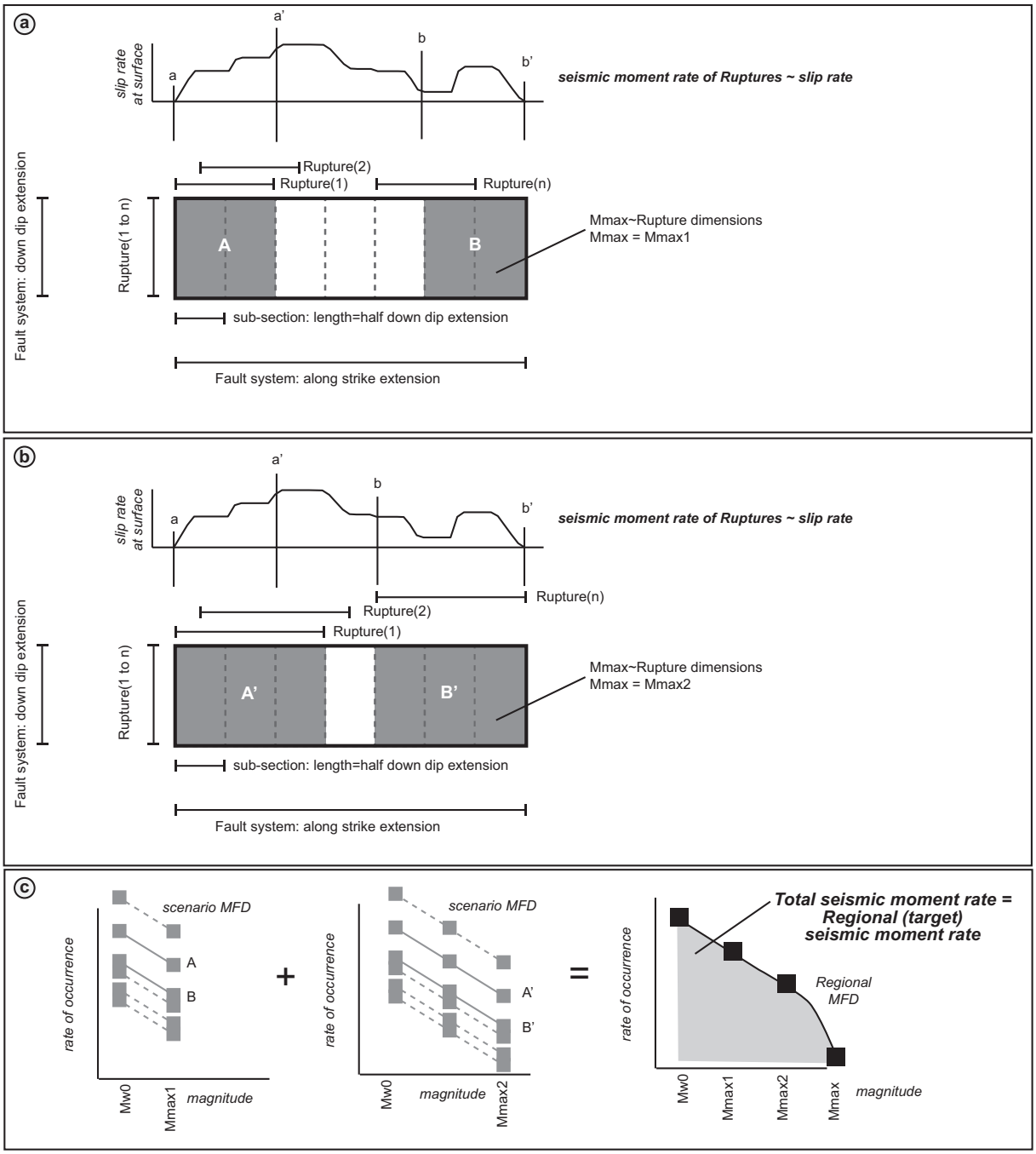


*FIG. 2. SUNFiSH approach. 2a) sketch of a fault plane to illustrate sub-sections and some of the possible rupture- scenarios at the minimum of the maximum magnitudes (two of the possible scenarios are marked as "A" and "B", with 2 sub-sections). To each scenario, an average slip rate is assigned. The maximum magnitude of each scenario is Mmax1. 2b) same fault plane and sub-sections as in 2a, to illustrate scenarios involving 3 sub-sections (two of the possible scenarios are marked as "A" and "B", with 3 sub-sections). To each scenario, an average slip rate is assigned. The maximum magnitude of each scenario is Mmax2. 2c) MFDs of the possible rupture- scenario. For each scenario an MFD is imposed. The seismic moment rate obtained by the sum of all MFD is imposed to be equal to the regional target seismic moment rate*

## 3.2 FRESH: a floating-rupture approach

FRESH (*Floating-Rupture for Seismic Hazard*) was designed to solve for the long-term rate of every possible earthquake rupture (above a threshold magnitude, Mw 5.5 in this test case) on a fault or fault system. The first step is the definition of the fault source in terms of a fault trace and geometry at depth and upper and lower seismogenic depths. Adopting the approach used in OpenQuake to model complex faults ([37]), we defined a sequence of fault edges (longitude, latitude and depth) to model irregular fault planes, for instance, fault with a variation of dip and seismogenic thickness. Secondly, we defined a mesh to sample the fault plane (Fig. 3a), specifically the level of discretization of the mesh representing faults. This mesh is used to discretize the ruptures. We generated ruptures for each expected magnitude according to a magnitude–area scaling relationship ([26]), with an aspect ratio value (set to 1 in this test case), and placed them on all possible locations on the fault surface (Fig. 3a, b). Ruptures with a surface lower than the whole fault surface are floated so as to cover as homogeneously as possible the fault surface (Fig. 3a, b). In particular, for the test case illustrated in this work, we adopted a mesh grid size of 3.5 km, resulting in a total number of 1367 possible ruptures with a magnitude ranging from Mw 5.5 to Mw 6.5.

In this study, we consider all ruptures in the same way, whereby a value of slip rate given by the integral mean of the slip rate profile between two endpoints of the rupture (points *a* and *b* in Fig. 3a, b) is assigned (see Eq. 2). Potentially the code allows a slip function that may vary with depth, limiting surface slip rate profiles to ruptures with upper boundaries corresponding to the top of the fault source (ruptures indicated by [1, 1] to [1, *n*] in Fig. 3a, b). For ruptures that do not reach the top of the fault source, a different slip profile than that deduced from surface data may be imposed.

FRESH requires to define an aseismic factor distribution along strike and dip of the fault system, to account, for locked and unlocked portions of the investigated fault system (Fig. 3c). In this study, we used an aseismic (or creeping factor) equal to zero (all the slip is seismically released) uniformly distributed along strike and depth of the fault system. As for the slip rate, to each sub-set of ruptures, a value of aseismic factor given by the integral mean of the aseismic factor profile between two endpoints of the rupture (points a and b in Fig. c) was assigned.

The next step is to calculate the product of the slip rate and aseismic factors at each rupture. Successively, this product is normalized to obtain a coefficient representative of the earthquake productivity of each rupture. For example, given a set of ruptures with magnitude *m1*, with slip rates $sr_i$ and aseismic factors $cf_i$, we compute a coefficient representative of the long-term rate of each rupture (*ki*). *Ki* is normalized by the sum of the *k* of all the possible ruptures (1 to *n*) with magnitude *m1*:

$$K_i = \frac{(sr_i\, cf_i)}{\sum_1^n (sr_j\, cf_j)} \qquad (6)$$

The last step of this approach is to link the coefficients $k_i$ to the target annual rate of occurrence (Fig. 3d). Starting from the target seismic moment rate, b and Mmax defined in section 2, and assuming a truncated-GR MFD, we compute the annual rate of occurrence for magnitudes greater or equal than the threshold Mw 5.5. To solve for the long-term rate of earthquakes for

the *i*th rupture ($\dot{Rup}$) of a certain magnitude (for example *m1*), we multiply the coefficient $k_i$ by the corresponding annual rate for that magnitude bin ($\dot{m}1$):

$$\dot{Rup}_i = k_i \dot{m}1 \qquad (7)$$

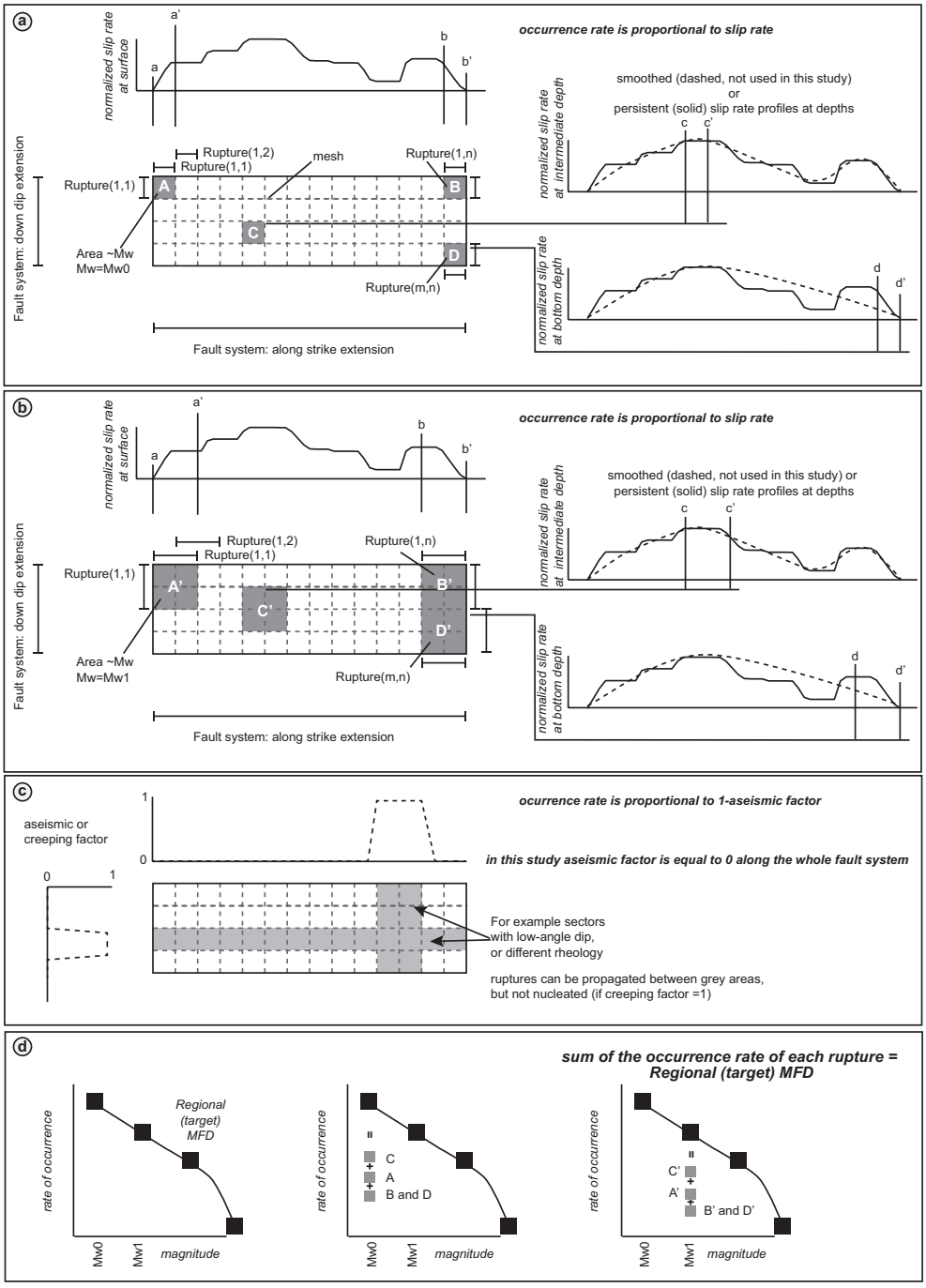


*FIG. 3. FRESH approach. 3a) sketch of a fault plane to illustrate the mesh grid, the floating ruptures and some of the possible ruptures at the minimum magnitude (ruptures marked with "A", "B", "C" and "D"). The magnitude of each rupture is Mw0. To each rupture, an average slip rate is assigned. 3b) same fault plane as in 3a, to illustrate ruptures with magnitude higher*

*than Mw0. The maximum magnitude of each scenario is Mw1. To each rupture, an average slip rate is assigned. 3c) Aseismic factor variations along strike and dip of the fault plane can be modelled by FRESH. In this study we used an aseismic factor equal to 0. 3d) A regional MFD is imposed. The sum of the rates of occurrence of each rupture is equal to the regional target MFD.*

### 3.3 SHERIFS

SHERIFS (*Seismic Hazard and Earthquake Rate In Fault Systems*) is an open-source python code to build hazard models allowing earthquake ruptures involving several fault sections (or Fault-to-Fault FtF ruptures). SHERIFS contains tools to calculate the annual rate of FtF ruptures and background seismicity rate as well as to set up and to weight the logic tree exploring a wide range of epistemic uncertainties.

SHERIFS applies the methodology presented in [14] to calculate the annual rates of earthquake on faults, which are computed following two constraints: the magnitude frequency distribution (MFD) of earthquakes in the fault system as a whole must follow an imposed shape and the rate of earthquakes on each fault is determined by the specific slip-rate of each section depending on the possible FtF ruptures. In the SHERIFS methodology, the shape of the MFD of each individual faults is not imposed and can differ from the shape of the MFD of the entire system. Relaxing the MFD shape at the section level allows respecting the slip-rate measured locally on the fault section. In order to comply with the MFD shape imposed for a fault system, SHERIFS may require to consider part of the fault slip-rate as aseismic. In the FRESH and SUNFiSH methodologies, an alternative choice is made whereby the slip rate is averaged over several sections for the larger ruptures in order to maintain the imposed regional (in FRESH) and scenario (in SUNFiSH) MFD shape.

Once geometries, slip-rate of the faults, possible FtF scenarios in the model and the shape of the regional MFD target are set, SHERIFS converts the slip-rate budget of each fault in earthquake rates following an iterative process that randomly selects different rupture scenarios. Rupture scenarios may be composed of both single fault and complex fault ruptures. The absolute value of the target MFD, unknown at the beginning of the iterative process, can be set in two ways: (i) once the budget of the faults participating in the larger magnitude earthquake is exhausted because at that moment the rate of the larger magnitude earthquakes is known, or (ii) if the iterative process reaches a point where the remaining moment rate in the system is just sufficient to complete the target shape in the lower magnitude range.

In the present exercise, no background seismicity is considered, thus SHERIFS attempts to adjust the regional MFD target by converting 100% of the fault geologic slip-rate into seismic moment rate and therefore earthquake rate. In turns out that in this specific exercise, SHERIFS did not require to consider parts of the fault slip-rate as aseismic, as in FRESH and SUNFiSH (note that in this study, FRESH and SUNFiSH considered all the slip is seismically released). Finally, no epistemic uncertainties were considered in this study. SHERIFS can calculate the rate of earthquakes for magnitudes starting as low as magnitude 4 but in this exercise, the minimum magnitude was set at 5.5 in order to be compatible with the other approaches.

## 4. Non-FtF approaches

In order to show the impact of multi-fault rupture approaches including slip rate variability along a fault system, we compared SHERIFS, SUNFiSH and FRESH approaches, with two standard approaches, respectively a strictly-segmented fault source based on data from the individual seismogenic sources (ISS) and an un-segmented seismogenic source (USS) with an average slip rate.

According to [4] and [5], an ISS represents a fault that can break entirely during an earthquake. The ISS fault source input was built using the seven individual seismogenic sources depicted in Figure 1, with Mmax and slip rates are given in the table in Figure 1. For each of these fault sources, we computed a seismic moment rate by using equation 2. This value of seismic moment rate was then used to compute the activity rates for magnitudes from Mw 5.5 to the Mmax by assuming a Truncated-GR MFD with b = 0.99. Summing the seismic moment at the maximum magnitude of the seven fault sources, we obtained a value of 1.95 E+16 $Nmyr^{-1}$.

As regards the USS fault source input, we started with the fault geometry defined in section 2, assuming an un-segmented fault with a length of ~180km along strike. Earthquake ruptures, similarly to SHERIFS, SUNFiSH and FRESH, were allowed to float along the whole surface. However, the main difference is that an average value of slip rate is used for this fault, similarly to the recent fault-based PSH models for Europe and Middle East ([38]; [39]). The total seismic moment rate was computed to be 3.29 E+16 $Nmyr^{-1}$. This value of seismic moment rate was used to compute the activity rates for magnitudes from Mw 5.5 to the Mmax Mw 6.5, assuming a Truncated-GR MFD with b = 0.99.

## 5. Results: Fault modelling for PSHA

### 5.1 From field data to slip in fault models

Figure 4 describes how slip rates were used by the five approaches.

In Figure 4a slip rates of the ISSs are plotted against the along-strike distance of the fault system. Along with the individuals slip rates, an interpolated slip rate profile is also shown. Starting from this interpolated slip rate profile, we compute an average (integral mean) slip rate, that is then used as input for the USS model (Fig. 4b).

The interpolated slip rate profile represents a common input for SHERIFS, SUNFiSH and FRESH, however, because the three approaches model slip rates differently (Figures from 4c to 4i) the interpolated slip rate profile is plotted along with the slip rates actually used by SHERIFS, SUNFiSH and FRESH to model rates of occurrences of earthquake ruptures.

For SHERIFS (Fig. 4c) each dot represents the slip rate of each scenario, the slip rate was taken as the value corresponding to the profile shown in Figure 3b in the centre of each scenario.

FRESH and SUNFiSH computed an integral mean of the slip rate for each rupture, starting from the interpolated slip rate profile included between the ends of the rupture. Because SUNFiSH used consecutive sections to model earthquake rupture from 5.5 to the maximum magnitude allowed by fault area, in Figures 3d, 3f and 3h we plotted the slip rate interpolated profile along with the average slip rate of the ruptures involving, respectively, 2, 4 and 7 sections.

FRESH is based on floating ruptures, whose area is derived from the magnitude. Slip rates of ruptures with Mw 5.5, 6.0 and 6.5 are plotted in Figures 4e, 4g and 4i.

As regards FRESH and SUNFiSH, it is important to note that the larger is the rupture, the smoother is the slip rate, however, all three approaches allow to reproduce the slip rate variability along strike, and consequently model variations of rates of occurrence of earthquake ruptures along the fault system, within a relaxed-segmentation framework. Conversely, with ISS and USS approaches, the slip rate variability or the un-segmented (floated ruptures along the whole fault system) were mutually exclusive.

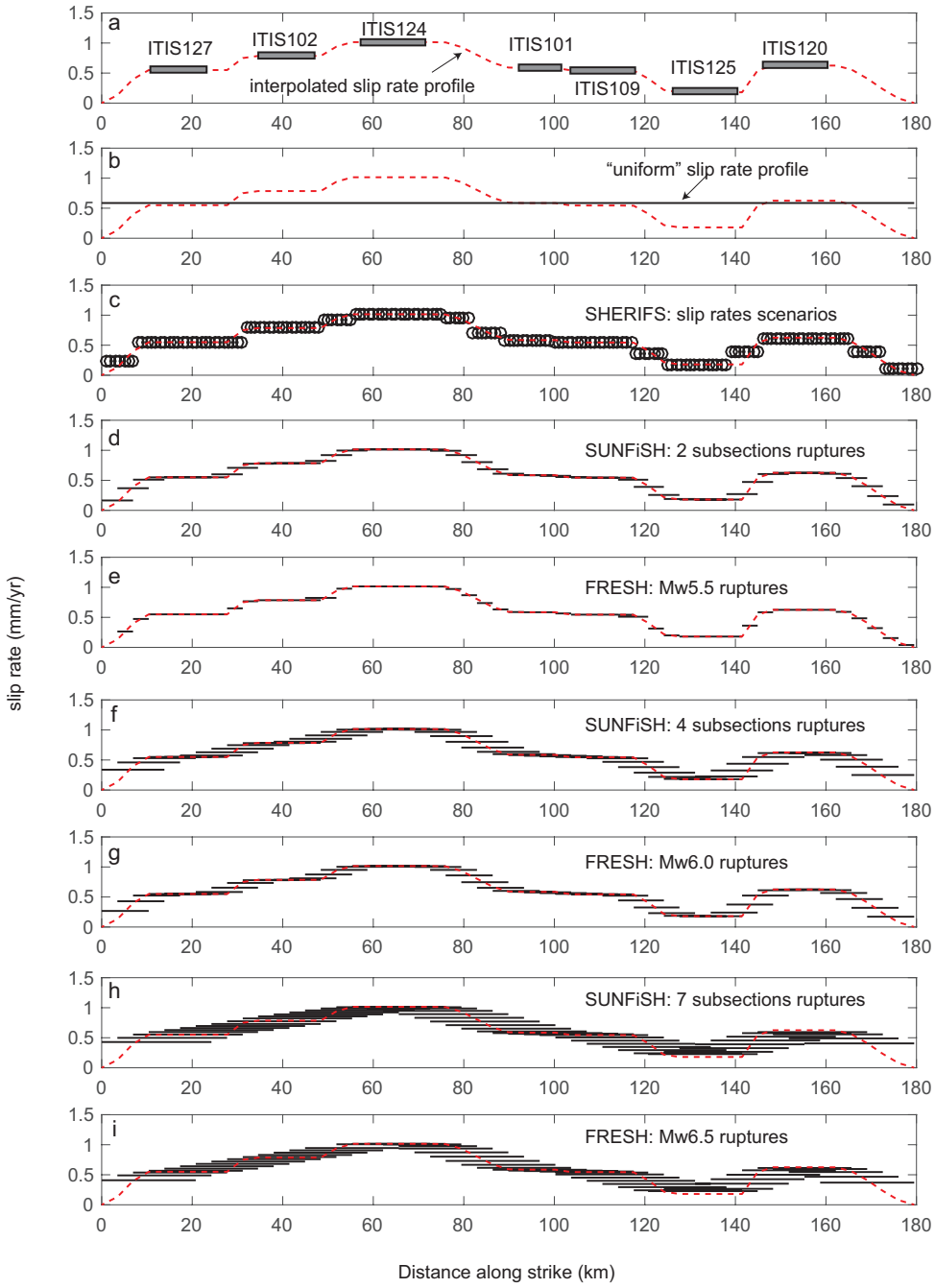


*FIG. 4. Slip rates. 4a) Slip rates from the ISS (grey rectangle), used in the ISS approach, and interpolated profile (red dashed line, the same in 4b-4i). 4b) Slip rate used in the USS approach. 4c)*

*SHERIFS: circle are the slip rates assigned to each scenario. 4d), 4f) and 4h) SUNFiSH slip rate calculated for each scenario (horizontal black lines), involving respectively, 2 (scenarios with the minimum number of sub-sections), 4 and 7 (scenarios with the maximum allowed number of sub-sections in this study). 4e), 4g) and 4i) FRESH slip rate calculated for each scenario (horizontal black lines), with ruptures of magnitude respectively, 5.5 (minimum magnitude in this study), 6.0 and 6.5 (maximum magnitude in this study).*

## 5.2 From slip in fault models to frequency-magnitude distributions

Figure 5 shows MFD modelled by the 3 approaches. While the approaches show different magnitude-frequency distributions in the five sub-regions (and in the total MFD), it is important to note that they have the same amount of seismic moment rate of 3.29e+16 $Nmyr^{-1}$ More in detail, in Figure 4, shows the cumulative rate of occurrence of possible ruptures, in the range of Mw from 5.5 to 6.5.

With FRESH, the shape of the MFD is defined at the fault system level and the approach allows to preserve this shape at the level of single sections: each rupture has a magnitude-rate pair, and the sum of the rates ensure the preservation of the input MFD at the fault system and section levels.

With the SUNFiSH approach, the MFD is defined at the level of sections: each combination of sub-sections has an MFD (in this case we used a classical GR), with a b value defined at the fault system level, and Mmax given by the number of sub-sections involved. Summing rates of sub-sections in a region or along the whole fault system does not ensure to preserve a target GR, only the total seismic moment rate is preserved.

With SHERIFS the MFD is defined at the fault system level in terms of b value, the Mmax is a result of combinations of sections imposed to rupture together. SHERIFS does not seek to preserve the shape of the regional MFD at the fault section level, as it depends on the aleatoric variability of modelled rupture occurrence.

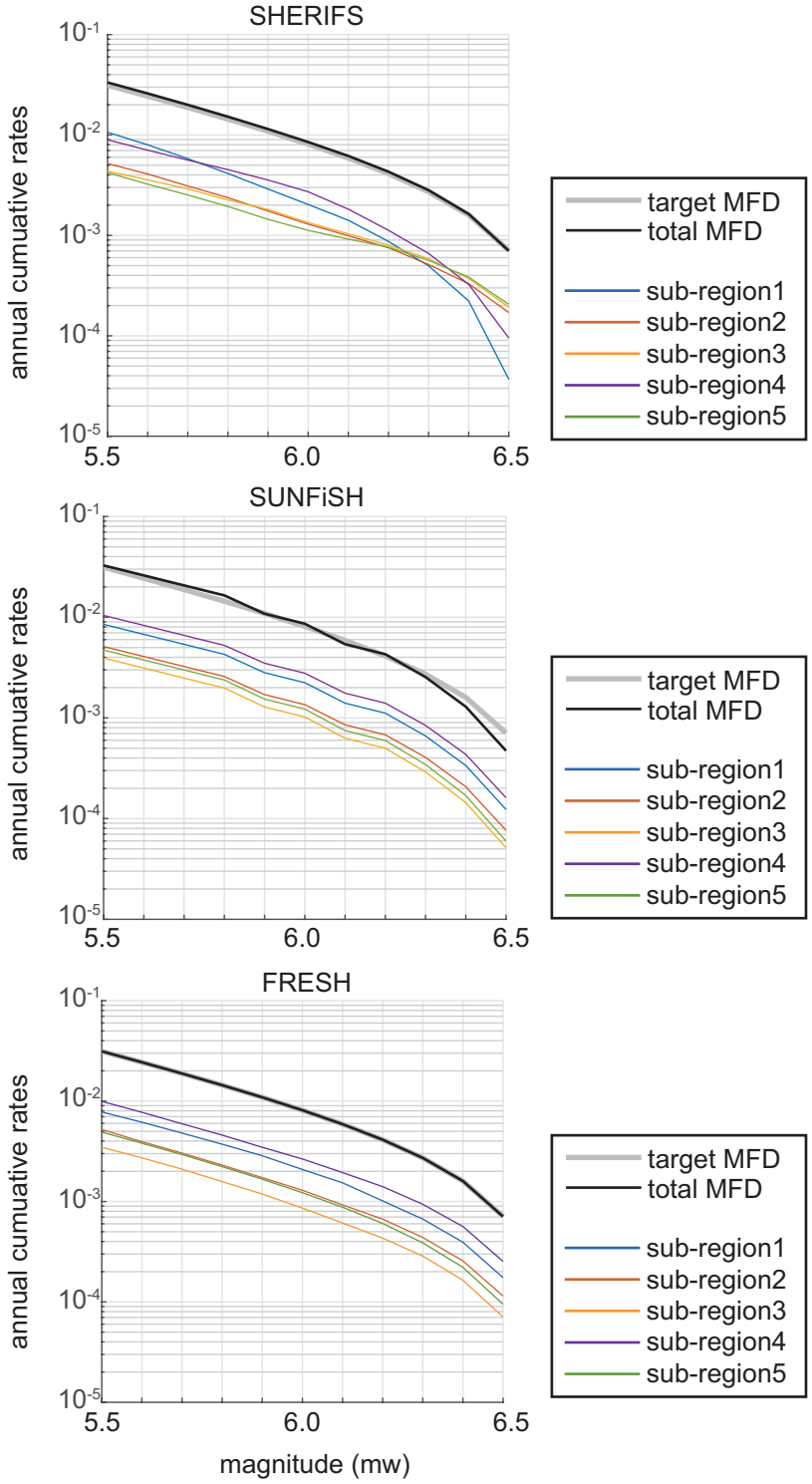


*FIG. 5. MFD from SUNFiSH, FRESH and SHERIFS in the 5 sub-regions. The target regional MFD used in SUNFiSH and SHERIFS is also shown.*

## 6 Discussions: From FMD to seismic hazard.

The resulting impact in terms of PSHA is shown in Figure 6 for peak ground accelerations (PGA) with 10% and 2% of probability of exceedance in 50 years computed with a ground motion prediction equation proposed by [40].

Not surprisingly, the main difference in PSHA among the 5 models is between the USS and the other four approaches. The use of an un-segmented fault data, with an average and unique slip rate, implies a uniform PGA distribution along the strike of the fault, with a maximum PGA value of ~0.35g and ~0.75g for the probability of exceedance of 10% and 2% in 50 years, respectively.

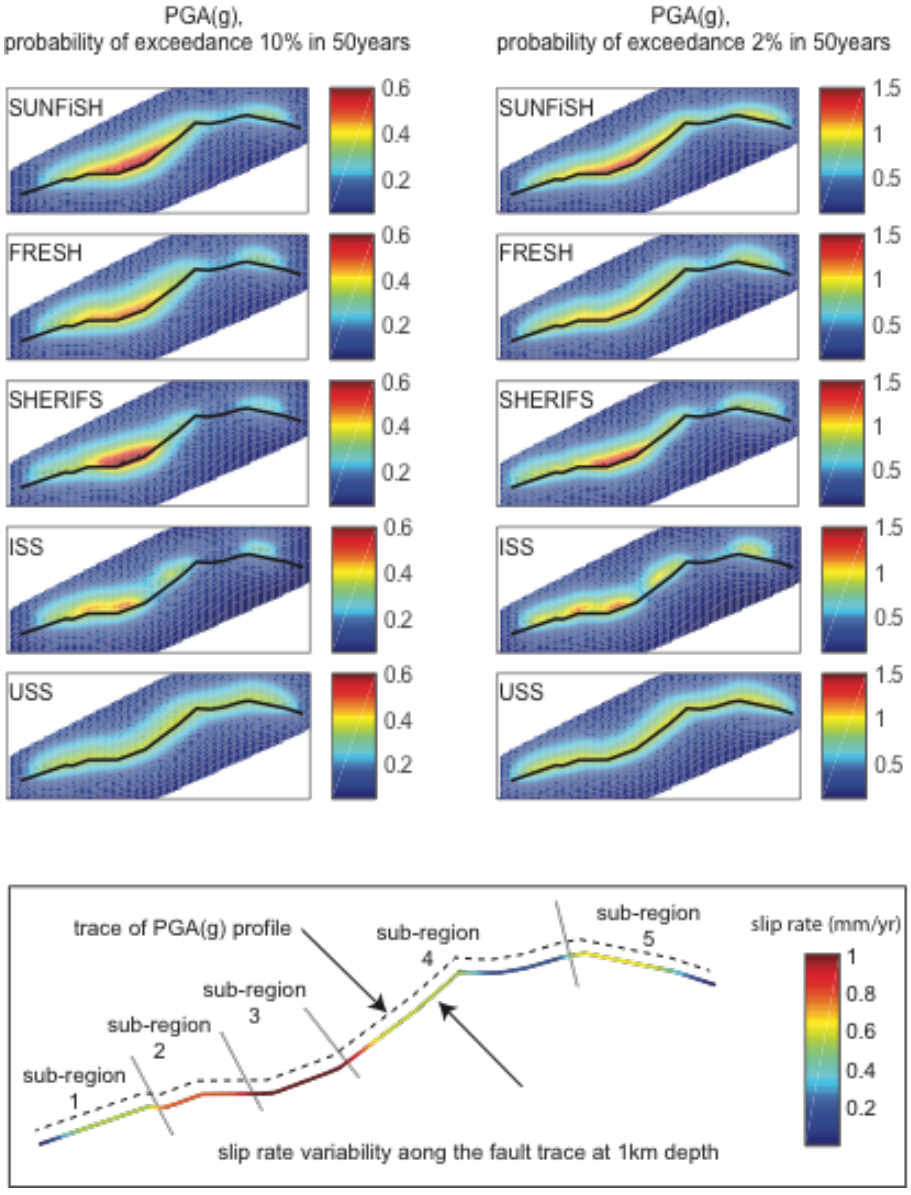


*FIG. 6. Maps of PGA (g) with the probability of exceedance of 10% (left column) and 2% (right column) in 50 years. In the bottom: fault trace with slip rate data (from the interpolated profile in fig. 4) and the trace of the profile used in figure 6. The 5 sub-regions discussed in the text are shown.*

The resulting PGA from ISS, SUNFiSH, SHERIFS and FRESH, on the other hand, show progressively higher values from the southwestern tip to the central-southeastern parts of the fault, that lead to the highest hazard levels. The PGA gradually diminishes towards the northeastern parts of the fault; a second area of relatively high PGA is observed in the northeastern part of the fault. Such a spatial pattern is observed for both probabilities of exceedance shown in Figure 6.

The effect of the segmentation is also shown in Figure 6, comparing hazard maps obtained from ISS with the others. In this case, the segmented model sub-region three and sub-region four show PGA values higher than the surrounding areas, in a spotted-pattern quite different from the un-segmented models. However, the ISS segmented model has some zero chance of observing a rupture, where the sources have not been identified along the fault system, leading to the segmented model being lower than the un-segmented model in three out of four cases (SUNFiSH, SHERIFS and FRESH), but in some areas higher than the USS.

To better understand the effects of segmentations vs multi-fault rupture models, we computed PGA profiles of the resulting PGA maps (Fig. 7), along a trace parallel to the top edge of the fault system at 1 km of distance from the top edge in the hanging-wall. As the USS, SUNFiSH, SHERIFS and FRESH models include a higher number of earthquake ruptures, continuously distributed along the fault system, it might intuitively suggest higher seismic moment rate, and in turns higher seismic hazard, than the ISS. In Figures 6 and 7, we show that the hazards derived from these un-segmented models are in fact generally higher with respect to the ISS values throughout the profile. In particular, in the region of maxima PGA, ISS returns PGA lower than FRESH, SUNFiSH and SHERiFS ones, in a range from ~5% up to ~37%. In the area of the minima PGA, ISS returns values lower than the FRESH, SUNFiSH and SHERiFS ones in a range from ~5% up to ~100%. The easternmost and westernmost ends of the sub-regions 1 and 5 are the areas where all the models are more in agreement, whereas the central part of the profile, and in particular in the sub-regions 3 and 4, the models show the highest differences. In these sub-regions, in fact, the USS shows an almost uniform PGA of ~0.35g, whereas, SUNFiSH, SHERIFS and FRESH indicate PGA values between ~0.45g and ~0.6g (~28% - ~70% difference) in sub-region 3, and PGA lower than the values obtained by the USS in the central-to-eastern part of sub-regions 4. Differences in PGA among FRESH, SUNFiSH and SHERIFS are generally lower than 30%, ~35% in the subregion3. It is worth noting that such differences depend on the probability of exceedance and on the ground motion predictive equation used. The aim of FRESH, SUNFiSH and SHERIFS is to model variation of slip rate and include FtF ruptures. As shown in Figures 6 and 7, the comparison with “strictly-segmented” or “un-segmented” approaches is not straightforward: increase or decrease in the hazard levels are not systematic. However FRESH, SUNFiSH and SHERIFS allow to draw patterns of seismic hazard which closely reflect the slip rate data provided by geologist. In particular, in Figure 6, slip rate variations along strike (slip rate profile in Fig. 4a) is shown along the trace of the fault. The first highest absolute differences in the expected PGA results (sub-region 3) between the multi-fault ruptures group of models and USS and ISS coincide with an area where the highest slip rates have been estimated, the second highest one (sub-region 4) is where the faults have the slowest slip rate estimates. In cases like this one, where fault slip rates were locally evaluated along a complex fault system, we consider it appropriate to apply multi-fault rupture models and possibly avoid uniform slip rate model. It is clear that multi-fault procedure requires a high level of knowledge and expertise in active tectonics, but averaging slip rates or building independent and strictly segmented models do not adequately reproduce available (and independent) data. This should be considered as a critical aspect when using fault-based models for PSHA.

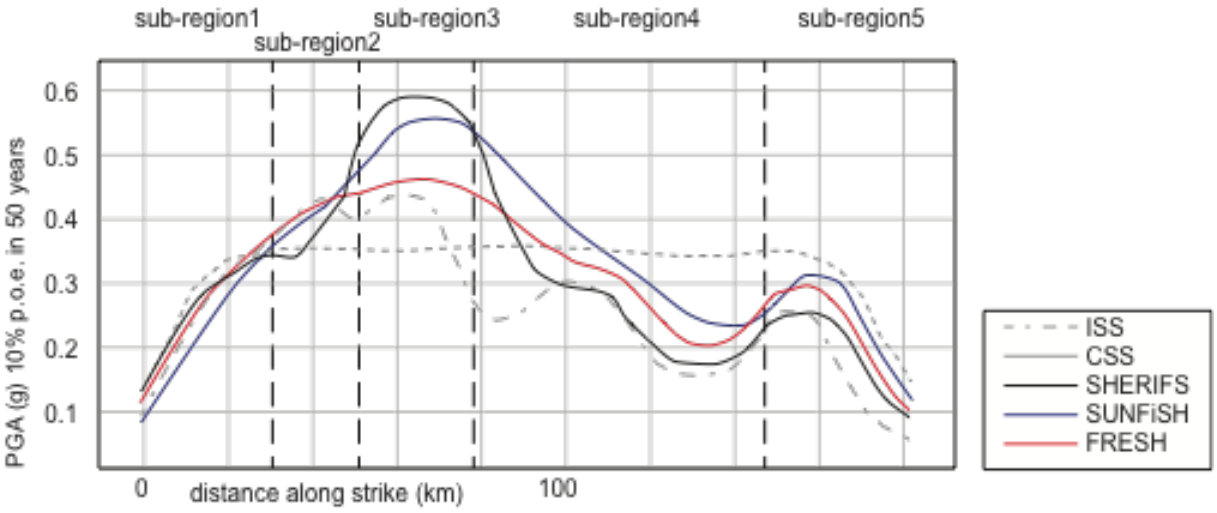


*FIG. 7.Profiles of PGA (g) with the probability of exceedance of 10% in 50 years. The 5 sub-regions discussed in the text are shown.*

The effect of modelling multiple-ruptures is shown in Figure 8, comparing the seismic moment rate distribution and earthquake rates-frequency distributions in the five sub-regions for the three models SUNFiSH, SHERIFS and FRESH. To build these distributions, we extracted rates and magnitudes of the ruptures completely included in the regions, and, for ruptures crossing boundaries of the sub-regions, we computed the amount of earthquake rates proportionally to the length of ruptures included in a sub-region. In terms of seismic moment rate distributions, in sub-regions 1 and 2, the differences are mainly at the highest magnitudes, which do not contribute much to the hazard levels computed here, having considered the 10% and 2% of probability of exceedance. The same pattern was observed for sub-region 5. Sub-regions 3 and 4 show the most interesting feature concerning the comparison between the resulting PGA and seismic moment rate distributions. In sub-region 3, SHERIFS methodology is computing the highest seismic moment rates, except for two magnitude bins at 5.8 and 6.0, where SUNFiSH has the highest values. In terms of PGA (profile in Fig. 6) in sub-region 3, the highest values are given by the SHERIFS methodology, the lowest by FRESH. In sub-region 4, the model returning the highest PGA is SUNFiSH, whereas the lowest values are from SHERIFS. Looking at the seismic moment rate distributions in Figure 8, we observe that the SUNFiSH approach leads to generally higher values compared to FRESH and SHERIFS in the range of magnitude 5.5-5.8 and for magnitude higher than 6.2. The difference between seismic moment rates distributions and the resulting PGA maps and profiles should be sought for in the modelling MFD of earthquake ruptures (Fig.5).

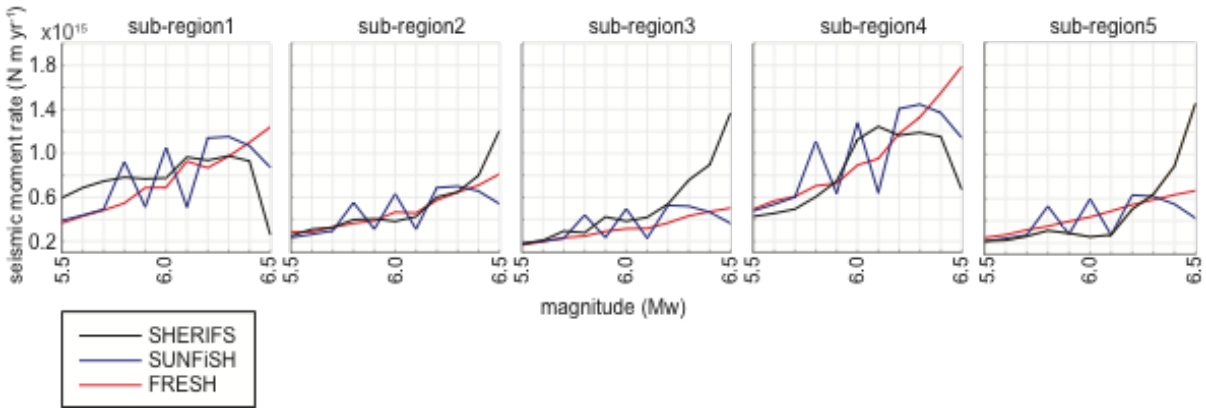


*FIG. 8. Seismic moment rate –magnitude distributions for the 5 subregions*

Beyond the PGA evaluated by the used approaches, the aspect that we consider important to highlight is: a) the USS model does not allow to consider the variability of the geological data, in this study, for example, the slip rate; b) the ISS model does not go beyond the known geological data and, therefore, does not allow to model complex ruptures (e.g., FtF), which would always be "surprising events"; c) the FRESH, SUNFiSH and SHERIFS models allow to consider the variability and complexity of the geological data and to model them to obtain PSHA estimates anchored to these data. Each of these methods (FRESH, SUNFiSH and SHERIFS) has advantages and limitations that depend on how it treats the input data (Table 2). The choice of one of the three methods could depend on the level of knowledge of the geology and tectonics of the study area. For example, having few spotted evidences of individual faults in a region, SHERIFS allows to use them as input and model multi-fault ruptures without extrapolating or interpreting data. On the contrary, in areas where long fault system, as for example a thrust front along a chain, without evidence of fault bends and ends, FRESH and SUNFiSH could allow to solve for possible multi-fault ruptures. In principle, there are no indications to prefer one model or another, and a weighted approach to combine them should be preferred.

| | ***FRESH*** | ***SUNFISH*** | ***SHERIFS*** |
|---|---|---|---|
| Input data + Procedure | Moment rate in the fault system; MFD for the fault system; Define floating ruptures by OpenQuake; rupture area proportional to magnitude; compute normalized coefficients of activity rates for each rupture based on its averaged slip rate (other constraints can be added); compute activity rate for each rupture by multiplying rate of the MFD at a given magnitude by the normalized coefficients for each rupure. | Moment rate in the fault system; For each possible rupture scenario averaged properties (slip rate and geometries) for that fault section are considered to compute activity rates from Mmin to Mmax following imposed MFD for each fault section. | Moment rate in the fault system; Compute activity rates for each fault in the system based on their individual slip rates and the set of fault-to-fault ruptures allowed in the system following imposed MFD in the fault system. |
| Fault to Fault rupture | Considered as aleatoric uncertainty | | |
| Mmax | Each rupture has a magnitude; Mmax of the fault system is imposed. | Each scenario has a maximum magnitude depending on the number of sections; Mmax of the fault system is imposed. | Calculated for each rupture. |
| Mmin | No limit, but below M5.5 many thousands of ruptures have to be managed and procedure may become cumbersome. | No limit. | No limit. |
| Complex Geometry | Possible. Ruptures on continuous surface. | Geometry of faults is averaged depending on faults involved in the rupture scenario (Faults need to be connected). | Possible - Faults may be disconnected. |
| Shape of target MFD | Defined at the fault system level and preserved at the section level. | Defined at the section level but not preserved at the fault system level. | Defined at the fault system level but not preserved at the fault section level. |
| Slip rate | Averaged and normalized for each floated rupture scenario. | Averaged for sections-rupture scenario. | Fault section specific . |
| Aseismic | 100% seismic (user can define variations of slip rates and aseismic portion along strike and depth of fault). | 100% seismic (user can define aseismic sections). | user can define aseismic sections In addition some % may be classed as NMS if initial moment rate cannot fit imposed regional target shape. |
| Epistemic Uncertainty exploration | Outside the code. | Outside of the code. | Within the code. |

*TAB. 2. Synoptic view of FRESH, SUNFiSH and SHERIFS approaches: key points of procedures and modelling of input data*

Finally, the recent evidences of earthquake occurrence, such as the 2012 Mw 8.6 Sumatra offshore earthquake, the 2016 Mw 7.8 Kaikōura earthquake, the Mw 6.5 2016 earthquake in central Italy and the Mw 6.5 2016 in Dartfield/Christchurch, required to question the relevance of segmenting fault system and, with this study, we started to investigate multi-fault rupture models. The case studied in this paper used simple assumption on the geometry of the fault system and the total seismic moment rate, but all three approaches allow to consider more complex geometries and include seismic moment rates obtained by non-geological data, for example from seismicity and geodesy, and are therefore useful tools that can be applied in a wide range of seismotectonic settings.

## 7. Conclusions

Our aim was to introduce a new objective and reproducible methodologies for evaluating the long-term rate of earthquake ruptures on a fault or fault system. The FtF approaches here presented are extensible to an entire fault system, with any kinematic and tectonic context. The test case here presented, as an application of the two methods, FRESH and SUNFiSH, compared with the already published SHERIFS FtF approach, allowed discussing implications of various assumptions in terms of PSHA. First of all, the question of how slip rate input data, often scattered along the fault system, can be modelled to define seismic moment rates long sections of a fault system. A second issue is the importance and the effect of boundaries constituting endpoints of ruptures, getting to the question of fault segmentation of primary relevance in the PSHA. As the first point of these approaches is to relax segmentation, the application of our methodologies requires to shift the paradigm from the individuation of earthquake rupture-barriers to the characterizations of FtF scenarios in fault systems. Applying our methodologies to an entire fault system allows capturing a larger number of possible ruptures than a segmented approach, and the PSHA reflects fault system geometry and slip rate distribution. However, all these approaches will never overcome the basic rule "trash-in, trash-out", especially for faults having little or no slip rate constraints. Future issues that need to be explored are the sensitivity of results given reasonable alternative values for the input parameters and choices. Ranking the 3 approaches to find a best, or a more useful, approach, is out of the scope of this paper: each method has advantages and limitations that depend on how it treats the input data (Table 2).

Finally, we summarize main results from our study:

a) We can relax segmentation, using FtF ruptures model instead of individuating and parameterising individual seismogenic sources;

b) we can calculate the long-term rate of every possible earthquake rupture of an un-segmented fault model;

c) we propose two new approaches and compare them with SHERIFS: a unique input data set can lead to differences up to 30% in the estimated seismic hazard (here PGA for 10% and 2% of probability of exceedance in 50 years) due to different assumptions considered in the fault-to-sha model

d) the 3 approaches allow to better reflect the input data (slip rate, complex geometry) compared to strictly-segmented or un-segmented models.

## Data and Resources

All data used in this paper came from published sources listed in the references. The OpenQuake code [37]) is available from www.globalquakemodel.org/oq-getting-started. FRESH, SUNFiSH and SHERIFS are available by request to the authors.

## Acknowledgments

Authors warmly thanks the FAULT2SHA members group for fruitful discussion and suggestions on the overall complex fault topics. We also thank Graeme Weatherill for the help with the OpenQuake python tool to build ruptures for FRESH, and Pierfrancesco Burrato for the detailed information on the slip rate calculation and derivation. FV is supported by FIRS 2016 - Visini F. - 0865.054 and CPS funds. A.V. is supported by Department INGeo funds (I. Raffi, responsible for “fondi dottorato” fund). T.C. is supported by AXA Research Fund. B.P. is supported by Department DiSPUTer funds (B. Pace, responsible for “ex 60%” fund).

## REFERENCES

[1] FIELD, E. H., DAWSON, T. E., FELZER, K. R., FRANKEL, A. D., GUPTA, V., JORDAN, T. H., et al. (2009). Uniform California earthquake rupture forecast, version 2 (UCERF 2). Bulletin of the Seismological Society of America, 99(4), 2053–2107, doi:10.1785/0120080049.

[10] ZHANG, H. & GE, Z. (2014). Rupture pattern of the Oct 23, 2011 Van-Merkez, Eastern Turkey earthquake. Earthquake Science 27: 257. https://doi.org/10.1007/s11589-014-0070-3.

[11] QUIGLEY, M., VAN DISSEN, R., LITCHFIELD, N., VILLAMOR, P., DUFFY, B., BARRELL, D., et al. (2012). Surface rupture during the 2010 Mw7.1 darfield(canterbury) earthquake: Implications for fault rupture dynamics and seismic-hazard analysis. Geology, 40(1), 55–58, doi:10.1130/G32528.1

[12] CHELONI, D., DE NOVELLIS, V., ALBANO, M., ANTONIOLI, A., ANZIDEI, M., ATZORI, S., et al. (2017). Geodetic model of the 2016 Central Italy earthquake sequence inferred from InSAR and GPS data. Geophysical Research Letters, 44(13), 6778–6787, doi:10.1002/2017GL073580.

[13] HAMLING, I. J., HREINSDÓTTIR, S., CLARK, K., ELLIOTT, J., LIANG, C., FIELDING, E., et al. (2017). Complex multifault rupture during the 2016 Mw7.8 Kaikōura earthquake, New Zealand. Science, 356(6334), doi:10.1126/science.aam7194.

[14] CHARTIER, T., SCOTTI, O., LYON-CAEN, H., & BOISELET, A. (2017). Methodology for earthquake rupture rate estimates of fault networks: Example for the western Corinth rift, Greece. Natural Hazards and Earth System Sciences, 17(10), 1857–1869, doi:10.5194/nhess-17-1857-2017.

[15] DOGLIONI, C., & BOSELLINI, A. (1987). Eoalpine and mesoalpine tectonics in the Southern Alps. Geologische Rundschau, 76(3), 735–754, doi:10.1007/BF01821061.

[16] CASTELLARIN, A., CANTELLI, L., F ESCE, A. M., MERCIER, J. L., PICOTTI, V., PINI, G. A., et al. (1992). Alpine compressional tectonics in the Southern Alps. Relationships with the N-Apennines. Annales Tectonicae.

[17] GALADINI, F., POLI, M. E., & ZANFERRARI, A. (2005). Seismogenic sources potentially responsible for earthquakes with $M \geq 6$ in the eastern Southern Alps (Thiene-Udine sector, NE Italy). Geophysical Journal International, doi:10.1111/j.1365-246X.2005.02571.x.

[18] SERPELLONI, E., ANZIDEI, M., BALDI, P., CASULA, G., & GALVANI, A. (2005). Crustal velocity and strain-rate fields in Italy and surrounding regions: New results from the analysis of permanent and non-permanent GPS networks. Geophysical Journal International, doi:10.1111/j.1365-246X.2005.02618.x

[19] ROVIDA, A., LOCATI, M., CAMASSI, R., LOLLI, B., & GASPERINI P. (2016). CPTI15, the 2015 version of the Parametric Catalogue of Italian Earthquakes, Istituto Nazionale di Geofisica e Vulcanologia, https://doi.org/10.6092/INGV.IT-CPTI15.

[2] STIRLING, M. MCVERRY, G., GERSTENBERGER, M., LITCHFIELD, N. VAN DISSEN, R., et al. (2012). National Seismic Hazard Model for New Zealand: 2010 Update. Bulletin of the Seismological Society of America, 102, 1514–1542,

doi:10.1785/0120110170

[20] SLEJKO, D., CARULLI, G. B., NICOLICH, R., REBEZ, A., ZANFERRARI, A., CAVALLIN, A., et al. (1989). Seismotectonics of the eastern Southern-Alps: a rieview. Boll Geof Teor App, 31, 109-136.

[21] POLI, M. E., PERUZZA, L., REBEZ, A., RENNER, G., SLEJKO, D., & ZANFERRARI, A. (2002). New seismotectonic evidence from the analysis of the 1976-1977 and 1977-1999 seismicity in Friuli (NE Italy). Bollettino di Geofisica Teorica ed Applicata, 43(1–2), 53–78.

[22] BASILI, R., VALENSISE, G., VANNOLI, P., BURRATO, P., FRACASSI, U., MARIANO, S., et al. (2008). The Database of Individual Seismogenic Sources (DISS), version 3: Summarizing 20 years of research on Italy's earthquake geology. Tectonophysics, 453(1–4), 20–43, doi:10.1016/j.tecto.2007.04.014.

[23] BURRATO, P., POLI, M. E., VANNOLI, P., ZANFERRARI, A., BASILI, R., & GALADINI, F. (2008). Sources of Mw5+ earthquakes in northeastern Italy and western Slovenia: An updated view based on geological and seismological evidence. Tectonophysics, 453(1–4), 157–176, doi:10.1016/j.tecto.2007.07.009.

[24] WEICHERT, D. H. (1980). Estimation of the earthquake recurrence parameters for unequal observation periods for different magnitudes. Bulletin of the Seismological Society of America, 70(4), 1337–1346, doi:10.1017/CBO9781107415324.004.

[25] STUCCHI, M., MELETTI, C., MONTALDO, V., CROWLEY, H., CALVI, G. M., & BOSCHI, E. (2011). Seismic hazard assessment (2003-2009) for the Italian building code. Bulletin of the Seismological Society of America, 101(4), 1885–1911, doi:10.1785/0120100130.

[26] WELLS, D. L., & COPPERSMITH, K. J. (1994). New Empirical Relationships among Magnitude, Rupture Length, Rupture Width, Rupture Area, and Surface Displacement. Bulletin of the Seismological Society of America, 84(4), 974–1002.

[27] PERUZZA, L., & PACE, B. (2002). Sensitivity analysis for seismic source characteristics to probabilistic seismic hazard assessment in central Apennines (Abruzzo area). Bollettino di Geofisica Teorica ed Applicata, 43(1–2), 79–100.

[28] BULL, J. M., BARNES, P. M., LAMARCHE, G., SANDERSON, D. J., COWIE, P. A., TAYLOR, S. K., & DIX, J. K. (2006). High-resolution record of displacement accumulation on an active normal fault: implications for models of slip accumulation during repeated earthquakes. Journal of Structural Geology, 28(7), 1146–1166, doi:10.1016/j.jsg.2006.03.006.

[29] NICOL, A., WALSH, J. J., VILLAMOR, P., SEEBECK, H., & BERRYMAN, K. R. (2010). Normal fault interactions, paleoearthquakes and growth in an active rift. Journal of Structural Geology, 32(8), 1101–1113, doi:10.1016/j.jsg.2010.06.018.

[3] PACE, B., PERUZZA, L., & VISINI, F. (2010). LASSCI2009.2: Layered earthquake rupture forecast model for central Italy, submitted to the CSEP project. Annals of Geophysics, 53(3), 85–97, doi:10.4401/ag-4847.

[30] D'AMATO, D., PACE, B., DI NICOLA, L., STUART, F. M., VISING, F., AZZARO, R., et al. (2017). Holocene slip rate variability along the Pernicana fault system (Mt. Etna, Italy): Evidence from offset lava flows. Bulletin of the Geological Society of America, 129(3–4), 304–317, doi:10.1130/B31510.1.

[31] ROBINSON, R., NICOL, A., WALSH, J. J., & VILLAMOR, P. (2009). Features of

earthquake occurrence in a complex normal fault network: Results from a synthetic seismicity model of the Taupo Rift, New Zealand. Journal of Geophysical Research: Solid Earth, 114(12), doi:10.1029/2008JB006231.

[32] COWIE, P. A., ROBERTS, G. P., BULL, J. M., & VISINI, F. (2012). Relationships between fault geometry, slip rate variability and earthquake recurrence in extensional settings. Geophysical Journal International, 189(1), 143–160, doi:10.1111/j.1365-246X.2012.05378.x.

[33] VISINI , F. & PACE, B. (2014). Insights on a Key Parameter of Earthquake Forecasting, the Coefficient of Variation of the Recurrence Time, Using a Simple Earthquake Simulator. Seismological Research Letters, 86, 703–713, doi: 10.1785/0220130165.

[34] PACE, B., VISINI, F., & PERUZZA, L. (2016). FiSH : MATLAB Tools to Turn Fault Data into Seismic-Hazard Models. Seismological Research Letters, 87(2A), 374–386, doi:10.1785/0220150189.

[35] HANKS, T. C., & KANAMORI, H. (1979). A moment magnitude scale. Journal of Geophysical Research B: Solid Earth, 84, 2348–2350, doi:10.1029/JB084iB05p02348.

[36] PAVLIDES, S., & CAPUTO, R. (2004). Magnitude versus faults' surface parameters: Quantitative relationships from the Aegean Region. Tectonophysics, 380(3–4), 159–188, doi:10.1016/j.tecto.2003.09.019.

[37] PAGANI, M., MONELLI, D., WEATHERILL, G., DANCIU, L., CROWLEY, H., SILVA, V., et al. (2014). OpenQuake Engine: An Open Hazard (and Risk) Software for the Global Earthquake Model. Seismological Research Letters, 85(3), 692–702, doi:10.1785/0220130087.

[38] WOESSNER, J., LAURENTIU, D., GIARDINI, D., CROWLEY, H., COTTON, F., GRÜNTHAL, G., et al. (2015). The 2013 European Seismic Hazard Model: key components and results. Bulletin of Earthquake Engineering, 13(12), 3553–3596, doi:10.1007/s10518-015-9795-1.

[39] DANCIU, L., ŞEŞETYAN, K., DEMIRCIOGLU, M., GÜLEN, L., ZARE, M., BASILI, R., et al. (2017). The 2014 Earthquake Model of the Middle East: seismogenic sources. Bulletin of Earthquake Engineering, pp. 1–32, doi:10.1007/s10518-017-0096-8.

[4] PERUZZA, L., PACE, B., & VISINI, F. (2011). Fault-based earthquake rupture forecast in Central Italy: Remarks after the L'Aquila Mw 6.3 Event. Bulletin of the Seismological Society of America, doi:10.1785/0120090276.

[40] CAUZZI, C., FACCIOLI, E., VANINI, M., & BIANCHINI, A. (2015). Updated predictive equations for broadband (0.01–10 s) horizontal response spectra and peak ground motions, based on a global dataset of digital acceleration records. Bulletin of Earthquake Engineering, 13(6), 1587–1612, doi:10.1007/s10518-014-9685-y.

[5] VALENTINI, A., VISINI, F., & PACE, B. (2017). Integrating faults and past earthquakes into a probabilistic seismic hazard model for peninsular Italy. Natural Hazards and Earth System Sciences, 17(11), 2017–2039, doi:10.5194/nhess-17-2017-2017

[6] KING, G., & NABELEK, J. (1985). Role of Fault Bends in the Initiation and Termination of Earthquake Rupture. Science, 228(4702), 984–987,

doi:http://www.jstor.org/stable/1694250.

[7] SWAN, F. H., SCHWARTZ, D. P., & CLUFF, L. S. (1980). Recurrence of Moderate to Large Magnitude Earthquakes Produced by Surface Faulting on the Wasatch Fault Zone, Utah. Bulletin of the Seismological Society of America, 70(5), 1431–1462.

[8] SCHWARTZ, D. P., & COPPERSMITH, K. J. (1984). Fault behavior and characteristic earthquakes: Examples from the Wasatch and San Andreas Fault Zones. Journal of Geophysical Research: Solid Earth, 89(B7), 5681–5698, doi:10.1029/JB089iB07p05681.

[9] FIELD, E. H., ARROWSMITH, R. J., BIASI, G. P., BIRD, P., DAWSON, T. E., FELZER, K. R., et al. (2014). Uniform California Earthquake Rupture Forecast, version 3 (UCERF3) -The time-independent model. Bulletin of the Seismological Society of America, 104(3), 1122–1180, doi:10.1785/0120130164.